



Investigations on L-valine doped imidazolinium L-tartrate (IMLT) single crystals

P. Dhivya¹, Mitrabhanu Behera², and R. Arun Kumar^{2,*}

¹Department of Physics, PSGR Krishnammal College for Women, Coimbatore, India

²School of Sciences (Physics), National Institute of Technology Andhra Pradesh, West Godavari (DT), Tadepalligudem, Andhra Pradesh 534101, India

Received: 17 September 2022

Accepted: 28 October 2022

Published online:

7 January 2023

© The Author(s), under exclusive licence to Springer Science+Business Media, LLC, part of Springer Nature 2023

ABSTRACT

Single crystals of imidazolinium L-tartrate (IMLT) crystals and L-valine doped IMLT crystals, with good optical quality, were grown by using the versatile slow cooling solution growth technique, for opto-electronic applications. The grown crystals were subjected to powder X-ray diffraction technique and the diffraction peaks were indexed. The grown crystals exhibit the monoclinic crystal structure, with the lattice parameters of $a = 6.72 \text{ \AA}$, $b = 6.90 \text{ \AA}$, $c = 9.65 \text{ \AA}$, and $\alpha = \gamma = 90^\circ$, $\beta = 87.70^\circ$. The variations in the cell volume, lattice parameters, due to the doping of amino acid (L-valine) in three increasing dopant concentrations, were studied and the evolved strains were found to be tensile in character. The high transparency of the doped crystals was compared with that of the pure imidazolinium L-tartrate (IMLT), which demonstrates that the effect of dopant has enhanced the optical properties of the synthesized single crystals. The optical constant values such as bandgap energy and cut-off wavelength were also analyzed. The dielectric properties of the grown crystals i.e. the dielectric constant and dielectric loss were recorded at room temperature for both pure and L-valine doped IMLT single crystals, through which it is understood that 1 mol% L-valine doped single crystals have minimum power dissipation factor. By adopting the fourier transform infrared spectroscopic analysis the vibrational frequencies of carboxyl group and the vibrations of other intended functional groups were ascertained. The rectangular etch patterns were observed while etching the surface of the grown crystals with the water. The densities of the etch pits were found to be lesser for the 1 mol% L-valine doped single crystals when compared with other doped crystals. The existence of carbon, hydrogen and nitrogen was confirmed in the analytical carbon–hydrogen–nitrogen (CHN) study in both the doped and un-doped IMLT single crystals. It was also found that the existence of carbon, hydrogen and nitrogen have proportionally improved as the concentration of doping agent increases. The nonlinear absorption coefficient and nonlinear refractive index were estimated using the Z-scan analysis from which the third order nonlinear susceptibility was calculated.

Address correspondence to E-mail: arunkumar@nitandhra.ac.in; aruncgc@gmail.com

1 Introduction

Lasers have become a vital tool for modernizing the current science and research initiatives. They have wide range of applications in the field of entertainment, manufacturing, warfare (laser-guided weapons), construction, communication, education, robotics, automotive sector, aviation, and etc. Materials with superior optical qualities combined with appreciable chemical, thermal and physical stabilities are highly essential for developing devices to cater to the needs of the society.

Materials belonging to the two classes-organic and inorganic based structures and compounds are widely used in optical industries. In the present decade, highly stable, single phased inorganic polycrystalline phosphor nanomaterials with unique luminescent properties that emit visible light upon exposure to UV-visible or visible light have gained much attention world-wide [1–3]. It has vast applications in the fabrication of solid-state lighting devices. Phosphor-in-glass (P-i-G) material is a composite of inorganic phosphor materials and glass materials, which functions as color converters upon irradiation with high energy / high power electromagnetic (EM) waves. These P-i-G materials are very much used in fabrication of light emitting diodes (LED) and white LEDs [4].

Research on the study of non-linear optical effects was earlier focused solely on pure inorganic crystal systems and quartz was the first solid crystal to have demonstrated the second order NLO properties among the inorganic single crystals. Research on inorganic materials such as ammonium dihydrogen phosphate (ADP), potassium dihydrogen phosphate (KDP), lithium niobate (LiNbO_3), β -barium borate (BBO), potassium titanyl phosphate (KTP) and lithium tri borate (LBO) were grown by many research scientists in the past decades for NLO applications [5–8]. Inorganic NLO materials are essentially bonded through ionic and metallic bonding. Inorganic crystals possess high melting point and high degree of chemical inertness due to the strong bonds present in them. Hence, majority of the commercial frequency doublers and applications in photonic industry utilize inorganic materials. Among the inorganic materials, potassium di-hydrogen phosphate (KDP) is one of the popular nonlinear optical materials used for frequency doubling phenomena.

It is now best understood through a high quantum of research that organic single crystals possess unique opto-electronic properties compared to inorganic crystals [9, 10]. This may be attributed to the fact that the organic molecules possess delocalized electrons, namely, conjugated electron systems which exhibit various nonlinear responses such as second harmonic generation, third harmonic generation, Pockel's effect, Kerr effect and etc. The organic materials with intra-molecular charge transfer compounds exhibit large second-order nonlinear optical (NLO) effects. It is possible to control the absorption edges of intra-molecular charge transfer compounds by selecting a judicious combination of donor and acceptor atoms present in the crystal.

This indicates the possibility of increasing the conversion efficiency due to the phenomenon of nonlinear optics, though a suitable combination of chiral molecule with large dipole moment and an organic molecule with non-centro symmetric structure. Organic materials are perceived as being structurally more diverse and therefore are believed to have more tailorable properties compare to inorganic counterparts [11]. A wide variety of organic materials are being investigated for frequency doubling processes and applications world-wide.

The organic crystals for nonlinear optical applications are grown by low temperature solution growth technique by majority of researchers. The low temperature solution growth is a versatile technique to provide the necessary super-saturation that enables the growth of NLO single crystals with lesser availability of defects. Some of the advantages of these organic materials are their high flexibility in terms of molecular structure, high optical laser damage threshold (LDT), low cost, ease of synthesis and short response time to optical excitation.

In order to enhance further the nonlinear optical efficiency of organic materials and to overcome few shortcomings in their application potential, suitable dopants can be added to better their favorable properties. Organic molecules are linked relatively with strong hydrogen bond, which permits to build up novel-organic complex crystals with good chemical stability, high nonlinear and molecular engineering features [12]. The aggregates constructed using hydrogen bonds induce changes in the structural and functional properties of the material [13]. They exhibit wide transparency in the UV-Vis near IR region. Their molecular chirality enables high

nonlinear susceptibilities by which they have a significant impact in nonlinear optical applications [14].

Imidazolium L-tartrate is an attractive ferroelectric material that guarantees numerous applications in nonlinear optics. Imidazole is a widely used ligand in chemical and biological molecules [15]. L-tartaric acid is a naturally occurring organic bi-carboxylic acid capable of initiating multi-directional hydrogen and covalent bonding. The derivatives of imidazole have improved mechanical and thermal stabilities. In our previous papers, we have demonstrated the enhancements in the properties of imidazolium L-tartrate single crystals by doping with two different amino acids—L-histidine, and L-proline [16, 17]. The zwitter ionic nature is very common in all amino acids which turns them to be a neutral molecule [18].

The amino acid L-valine ($C_5H_{11}NO_2$) has attracted researchers from pharmaceutical and optical industries owing to its peculiar properties. It draws significant interest in biological industries since L-valine is used in the biosynthesis of proteins. The presence of α -amino group (which is in the protonated $-NH_3^+$ form under the given biological conditions), α -carboxylic acid group (which is in deprotonated $-COO^-$ form under the particular biological conditions), and a side chain isopropyl group. It is a part of the non-polar aliphatic amino acid. Since it is an essential amino acid for human beings, it signifies that the human body cannot synthesize this particular amino acid and hence it must be acquired by the consumption of proper diet. L-valine finds applications in the food industry in addition to its significance in the pharmaceutical sectors. The amino acid L-valine can adapt to a given chemical environment straight forwardly. The investigations on the growth and characterization of single crystals doped with L-valine are limited in reports and hence in the present study we have undertaken the systematic investigations on the L-valine is doped in IMLT single crystals and the effect on the dielectric, optical, structural properties were analyzed using various characterization techniques.

2 Experimental technique

2.1 Growth of single crystals

The flowchart depicting the process of single crystal growth of pure and L-valine doped IMLT single crystals are presented in Fig. 1. High pure chemicals (around 97%, Sigma–Aldrich) were employed in the process of growing the single crystals. Both imidazolium ($C_3H_5N_2^+$) and L-tartaric acid ($C_4H_6O_6$) were taken in stoichiometric ratio (equal molar concentration) and were blended in deionized water to initiate the growth of single crystals of imidazolium L-tartrate (IMLT) by solvent evaporation technique. Then the saturated solutions of 1 mol%, 3 mol% and 5 mol% L-valine doped IMLT single crystals were grown by dissolving them in deionized water. The saturated solutions were stirred well using magnetic stirrer for the homogenization of the solutions prepared. The prepared supersaturated solutions were kept for slow evaporation of the solvents present in them. The flawless seed crystals were selected and grown into bulk crystals by using slow cooling method as shown in Fig. 2. The mother solutions for the growth of un-doped and concentration of 1 mol% L-valine doped IMLT single crystals were maintained at 35 °C, in a temperature-controlled water bath. The seed crystal was suspended in the solution which was kept in the temperature-controlled water bath operating with an accuracy of ± 0.01 °C for initiating bulk crystal growth. By decreasing the water bath temperature at a rate of 1 °C/day, single crystals with

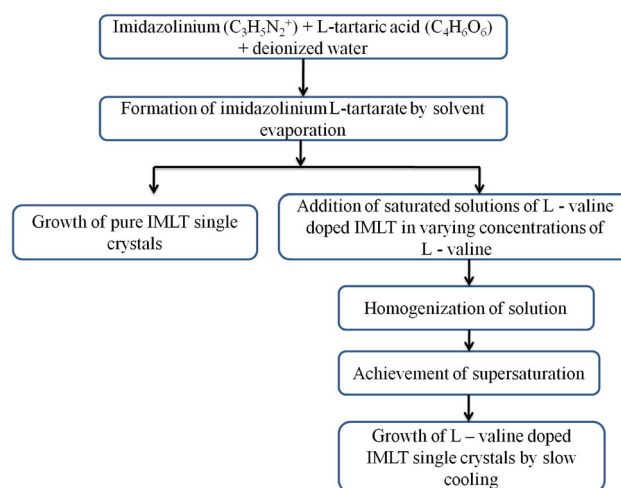


Fig. 1 Flowchart depicting the crystal growth process of pure IMLT single crystals and L-valine doped IMLT crystals

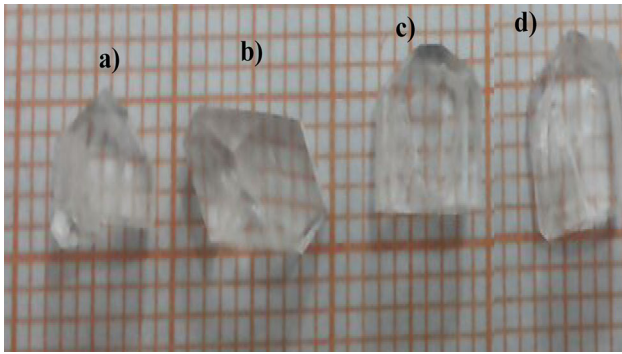


Fig. 2 Photographs of single crystals of **a** un-doped pure IMLT single crystal, **b** 1 mol%, **c** 3 mol%, **d** 5 mol% L-valine doped IMLT crystals

high optical qualities were harvested in duration of fifteen days. The same technique was implemented to grow the L-valine doped IMLT crystals pertaining doping concentration of 3 and 5 mol% respectively.

2.2 Characterization

Powder X-ray diffraction analysis was carried out with the help of Bruker D8 Advance powder X-ray diffractometer equipped with Cu-K α radiation of wavelength 1.5406 Å operated at a voltage of 45 kV and 30 mA current in the angular range (2θ) of 10–50°. Varian Cary 5000 Model spectrophotometer equipment was employed to perform the UV–Vis–NIR analysis. By using a Hioki 3532–50 LCR Hitester, in the frequency range from 50 Hz to 5 MHz, the dielectric measurements for the grown crystals were carried out. During the measurements, a coating of thickness 2 mm was made on the crystals with silver paste to impart conducting nature to the grown crystals. Elementar Vario EL III CHNS analyzer was used to study the proportions of carbon (C), hydrogen (H) and nitrogen (N) elements in the grown crystals. The IR spectrum was recorded using the IR tracer-100 (Shimadzu) spectrometer in the range of 400–4000 cm^{-1} by KBr pellet technique. Optical microscope BX53 Olympus was used to observe the etch patterns.

3 Results and discussions

3.1 Powder X-ray diffraction analysis

The characteristics of crystal structure were studied by PXRD analysis which was performed for the

powders obtained from the grown crystals and is shown in Fig. 3. Since a portion of the grown crystals harvested are powdered to carry out the analysis, all the essential information that are obtained by single crystal x-ray diffraction studies can be obtainable through the powder XRD analysis itself. The cell parameters and crystal structure were calculated using the unitCell software and are tabulated in Table 1. From the table it is observed that the crystal belongs to the monoclinic crystal structure. The sharp peaks denote that the grown crystals are highly crystalline in nature. All the grown crystals are isostructural in nature and no extra peaks were observed which confirms that no phase change has occurred due to doping [19]. The cell parameters are observed to be varied; this can be attributed the inclusion of the dopant L-valine in the IMLT crystals. The crystallite size obtained from the intensity data of few peaks such as (110), (011), (102) were found to increase with the increase in the dopant concentration as calculated using the Scherrer equation (Eq. 1). The value of full width at half maximum height (β) of the obtained XRD peaks, for the determination of crystallite size was obtained using the nonlinear Gaussian fit distribution function. The dislocation density gives an estimation of the amount of defects present in the crystal. Lesser the dislocations, the quality of the crystal is expected to be superior, and hence improved device performance. The strain (ϵ) and dislocation density (δ) were also calculated by using the formulae mentioned below (Eqs. 2, 3)

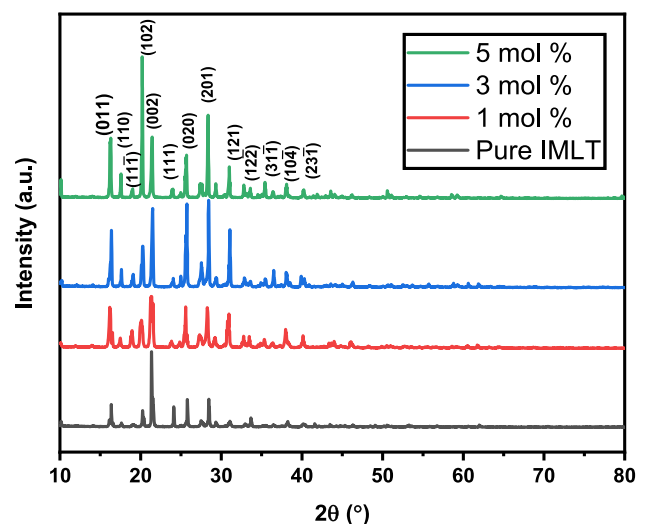


Fig. 3 Powder XRD pattern of pure and L-valine doped IMLT crystals

Table 1 Structural parameters (unit cell data) of pure IMLT and L-valine doped IMLT single crystals

Lattice Parameters	Pure IMLT	1 mol% LV doped IMLT	3 mol% LV doped IMLT	5 mol% LV doped IMLT
a (Å)	6.72	6.81	6.67	6.95
b (Å)	6.90	6.93	7.04	7.07
c (Å)	9.65	9.62	9.59	9.78
β (°)	87.70	88.41	88.92	90.36
α = γ (°)	90	90	90	90
Cell volume (Å) ³	451.8	469.41	473.46	484.16
Crystal structure	Monoclinic	Monoclinic	Monoclinic	Monoclinic

respectively and are furnished in Table 2. The strain developed due to the doping of amino acid L-valine is found to be tensile strain that makes vacancy type of defects [20]. It was found that the L-valine (LV) doped IMLT single crystal has the large crystallite size in the case of 1 mol % doping concentration. This implies that the atoms are well distributed [21]. From Fig. 4, it is detected that the 5 mol% L-valine doped IMLT crystal exhibits a particular peak with more intensity which implies that there is an extension of the surface of (102) plane. This is due to the fast growth rate of plane perpendicular with the introduction of 5 mol% L-valine as dopant [22]. It can be observed that the intensities of some peaks such as (111), (002) (020), (121) decrease which confirms the incorporation of dopants in the host (IMLT) single crystals and the impact is such that their morphology is varied only to a certain margin but their structure is not altered. The crystal structure of pure IMLT crystal is depicted in Fig. 5.

$$D = \frac{K\lambda}{\beta \cos\theta} \tag{1}$$

$$\lambda = 1.5406 \text{ \AA}$$

β = Full-width at half maximum height (rad),
 θ = Bragg's diffraction angle (°)

$$\epsilon = \frac{\beta}{4 \tan\theta} \tag{2}$$

β = Full width half maxima (rad),

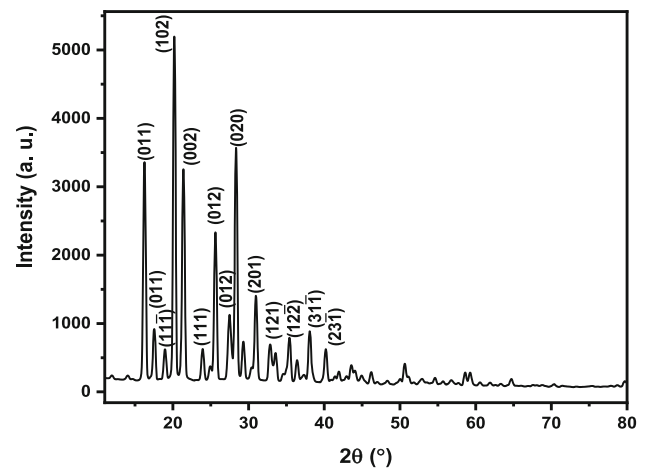


Fig. 4 PXRD pattern of L-Valine(5 mol%) doped IMLT single crystals

θ = Bragg's diffraction angle (°)

$$\delta = \frac{1}{D^2} \tag{3}$$

D = Crystallite size (nm).

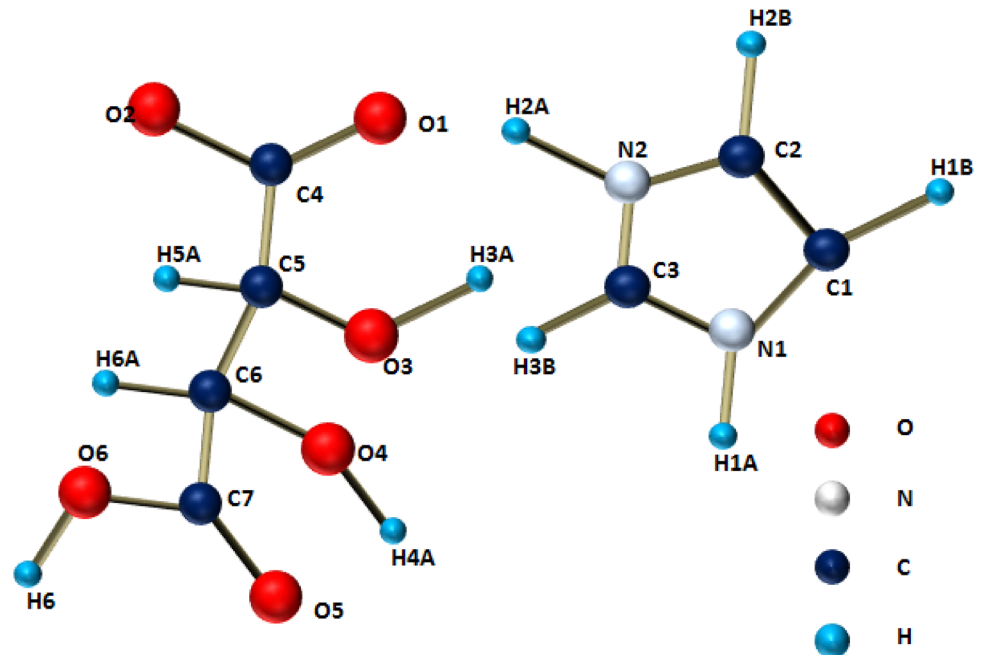
3.2 UV-Vis-NIR analysis

The optical spectrum analyses for the grown crystals were studied using the spectrometer operating in the absorption mode with the spectrometer. Grown crystals are expected to be highly transparent in the entire visible and near IR region for the practical use in NLO applications. This makes them suitable for

Table 2 Tabulation of crystallite size (D), strain (ε) and dislocation density (δ) of the grown single crystals

Crystal	Crystallite size (D) × 10 ⁻⁸ m	Strain (ε) (lin ⁻² m ⁻³) × 10 ⁻⁴	Dislocation density (δ) (lin m ⁻²)
Pure IMLT	5.32	17.45	1.8 × 10 ¹⁵
1 mol% LV	8.24	7.68	9.4 × 10 ¹⁴
3 mol% LV	5.61	8.46	9.0 × 10 ¹⁴
5 mol% LV	4.18	11.15	9.8 × 10 ¹⁴

Fig. 5 Crystal structure of pure IMLT crystal with the atomic position and numbering



applications in real-time devices. The transmission spectra are presented in Fig. 6 for the crystals grown. The output intensity of the transmission spectrum of L-valine doped crystals is found to increase upon doping which may be due to the decrease in the solvent inclusion and defects [23]. The active trapping of the impurities in the vacancies present in the IMLT crystals might have led to the decrease in the transmission of the pure crystals. These vacancies are filled by the dopant L-valine such that the defects get reduced and their output efficiency has increased

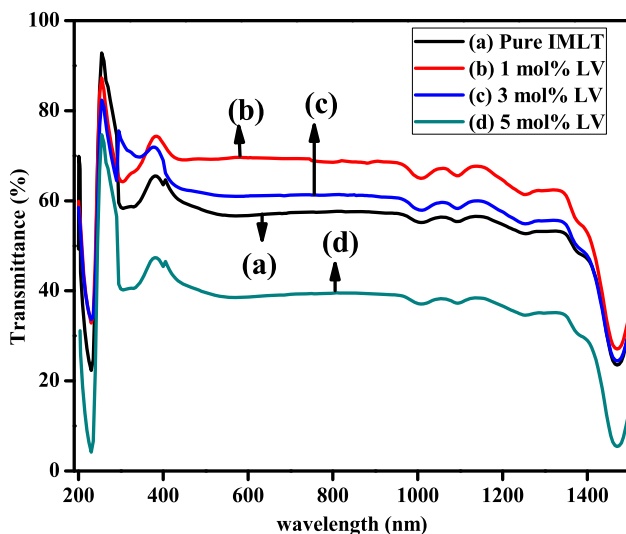


Fig. 6 Transmission spectra of undoped and L-valine doped IMLT single crystals

[24]. The cut off wavelength of the grown crystals were found and furnished in Table 3. The transparency and cut-off wavelength of the above-synthesized single crystals demonstrate their suitability in NLO applications. The decrease in the transmission around 234 nm and 331 nm is due to the transition of the orbital electrons i.e. $\pi-\pi^*$ and $n-\pi^*$ transitions in the grown crystals [25]. The Tauc's plot, plotted between $(\alpha h\nu)^{1/2}$ versus photon energy ($h\nu$) is shown in the Fig. 7 in the fundamental absorption region which is attributed to be indirect bandgap. The bandgap (E_g) was calculated by extrapolating the linear part of the plot between $(\alpha h\nu)^{1/2}$ versus ($h\nu$), which is based on the Tauc's equation (Eq. 4) and is presented in Table 3.

$$(\alpha h\nu) = K (h\nu - E_g)^n \quad (4)$$

α = Absorption co-efficient.

h = Planck's constant (6.627×10^{-34} m² kg/s).

ν = Frequency (Hz).

K = Energy independent constant.

E_g = Band gap.

n = Nature of transmission.

($n = 2$ for indirect band gap material).

($n = 1/2$ for direct band gap material).

It is to be mentioned here that various single crystalline materials also exhibit indirect electronic transition. Samples being crystalline in nature need

Table 3 The cut-off wavelength and optical band gap of the L-valine doped IMLT crystals

Crystal	Cut-off wavelength (nm)	Optical band gap E_g (eV)
Pure IMLT	263	4.72
1 mol % LV	257	4.82
3 mol % LV	259	4.79
5 mol % LV	260	4.76

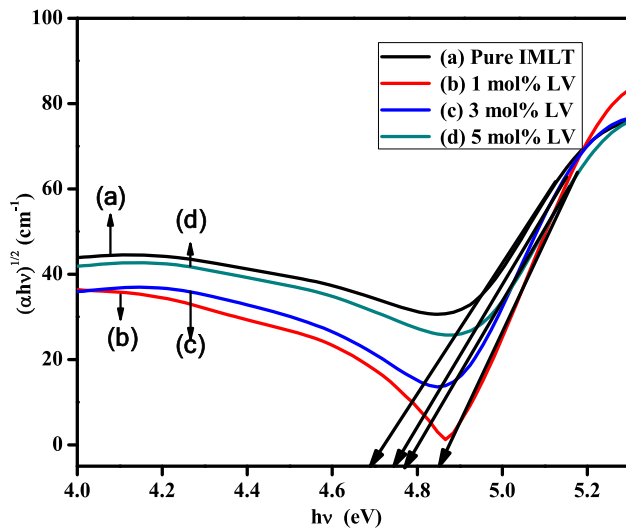


Fig. 7 Tauc's Plot of the pure and L-valine doped IMLT single crystals

not possess direct electronic transitions. These are placed with due respect to the journal.

3.3 Dielectric measurements

A dielectric material has the ability to dissipate minimum amount of heat energy and utilize the higher amount of energy for the dipole moment [26]. The crystal with minimum dielectric constant can be efficiently utilized since the dielectric loss can be minimized. The power dissipation is less in the dielectric material with minimum dielectric loss [27]. The basic mechanism of a dielectric material can be estimated by the decrement in its dielectric constant with an upon rising the applied frequency. This is due to the winding up of each polarization with the increase in frequency [28]. The polarization mechanism and the conduction process exhibit similarity. Each polarization disappears simultaneously as the frequency increases. Space-charge polarization will sustain only at low frequencies and vanishes as the frequency increases. Only electronic polarization exists at high frequencies and other polarizations i.e. ionic and orientation polarization disappear

gradually [29]. The dielectric constant for the grown crystals was calculated. The dielectric loss was also calculated. The obtained results are shown in Figs. 8, 9. The L-valine (1 mol%) incorporated IMLT crystals have low dielectric constant as well as low dielectric loss which implies that 1 mol% L-valine doping has minimum power dissipation and less heat energy loss compared with the all other grown crystals.

3.4 CHN elemental analysis

The CHN study affirmed the chemical proportion of these expected elements in both doped and un-doped IMLT single crystals. The recorded outcomes of the CHN analyses are furnished in Table 4, which presents a comparison between the experimental values and theoretical values. The formation of both doped and un-doped IMLT single crystalline compounds were validated and according to the comparison it was found that the experimental and calculated values of the expected elements (carbon, nitrogen and hydrogen) are in good agreement with one another. The proportion of existing carbon, hydrogen and nitrogen elements follow an increasing trend in as the concentration of dopant increases, which elucidates

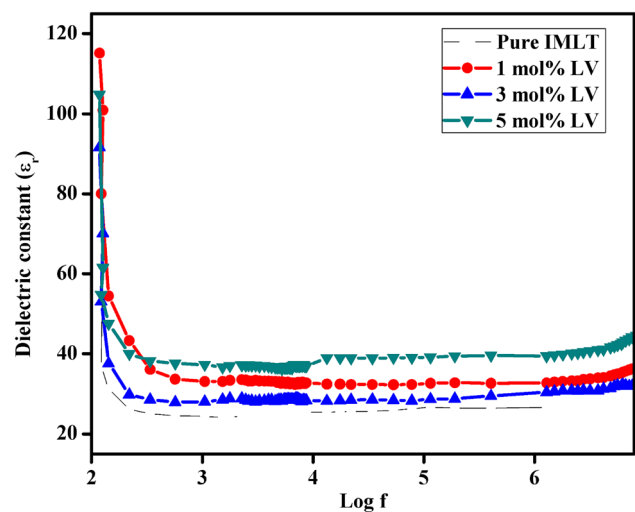


Fig. 8 Plot of dielectric constant Vs Log f

the presence of the dopant L-valine in the IMLT material.

3.5 FTIR analysis

Fourier transform infrared analysis (FTIR analysis) was recorded to analyze the functional groups present in the grown crystals. The IR spectra are shown in Fig. 10. The internal vibrations of the molecules were analyzed and the presences of hydrogen bonds within the spectrum in the grown crystals are furnished in Table 5. The functional groups and their bonding assignments confirms the presence of carbonyl group, C = O stretching, C–O stretching, O–H deformation [30] etc. The presence of the characteristic vibration of NH^{3+} in L-valine doped crystals and its absence in the spectrum of pure IMLT confirms the presence of amino acid (L-valine) in the doped crystals.

3.6 Etching studies

Etching is the reverse process of crystal growth mechanism [32]. When the surface of a crystal is etched with an etchant such as water or organic

solvents well—defined etch patterns are obtained. The distribution of structural defects can be investigated using the etching analysis. Etching analysis is a dominant tool to reveal the lattice inhomogeneities and dislocations that are present in grown crystals [31]. Etch pits can appear in various forms such as spirals, hillocks, rectangular etch pits, kinks, triangular etch pits and etc. In the present investigation, the grown crystals were subjected for etching by using water as an etchant and the etching time of about 10 s was maintained. The crystals were soaked in water for about 10 s, dried and were subjected to analyze the growth features. The morphology of the etch pits were studied in the reflection mode employing a metallurgical microscope. Etch pits in the form of rectangles were observed in the grown crystals and are shown in Fig. 11. Dislocations manifest to relax the stress created and reduce the lattice mismatch in the grown crystal [33]. Due to the inclusions of the dopants in the mother crystal, etch pits or dislocations are produced. It is expected that the air bubbles present in the grown crystals reduces its optical efficiency. From the Fig. 11, it can be observed that the etch pit densities are lesser in L-valine (1 mol%) doped IMLT single crystals whereas in pure un-doped IMLT and L-valine (5 mol%) doped IMLT single crystals, a large number

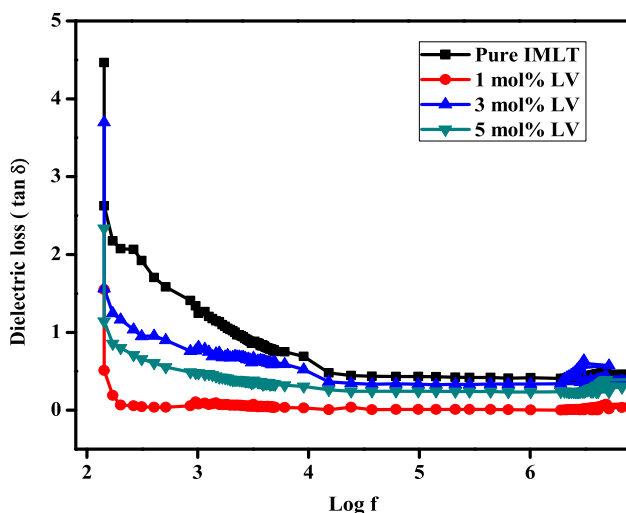


Fig. 9 Plot of dielectric loss Vs Log f

Table 4 CHN composition analysis of the grown IMLT single crystals

Element	Pure IMLT	Theoretical values (pure IMLT) (%)	1 mol% LV	3 mol% LV	5 mol% LV
C	38.62	38.50	38.81	39.05	39.11
H	4.40	4.5	4.51	4.58	4.48
N	12.67	12.8	12.71	12.80	12.89

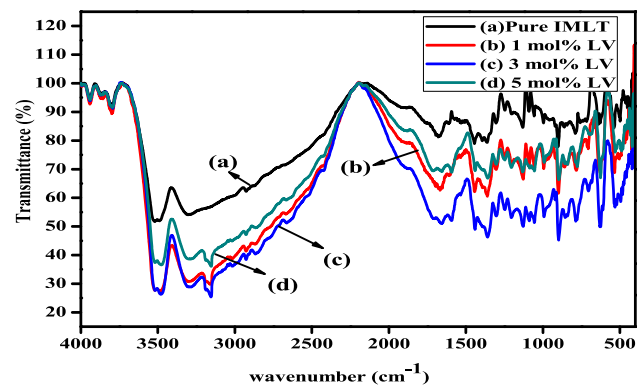
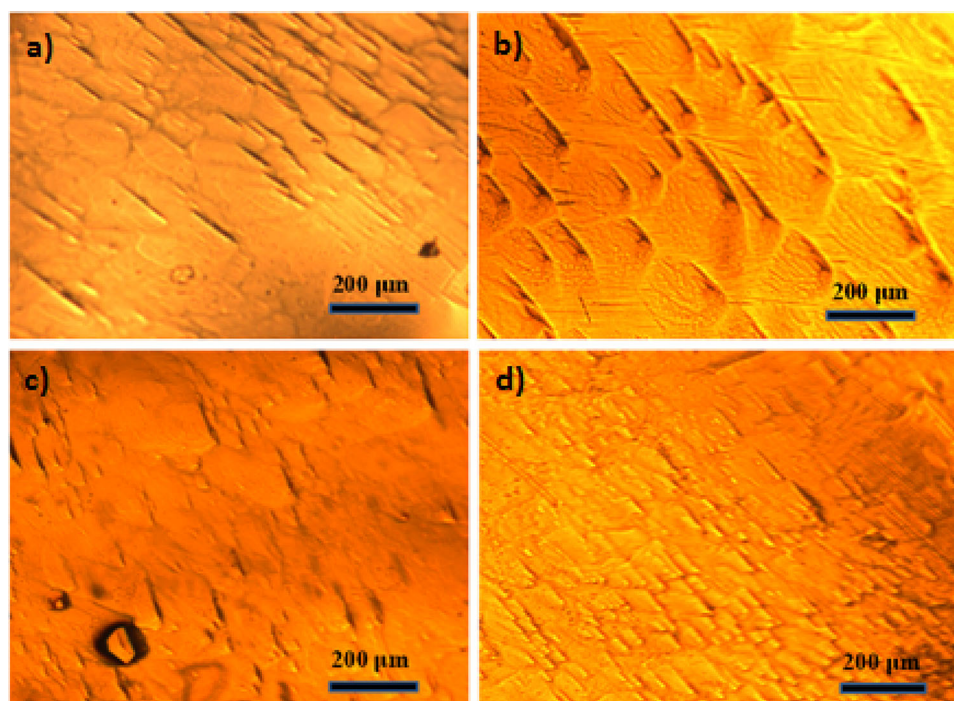


Fig. 10 FTIR spectra of grown single crystals. a Pure IMLT b 1 mol% L-valine doped IMLT c 3 mol% L-valine doped IMLT d 5 mol% L-valine doped IMLT

Table 5 FTIR spectral bond assignments in the grown single crystals

Absorption (cm^{-1})				Assignment of functional groups
Pure IMLT	1 mol% LV IMLT	3 mol% LV IMLT	5 mol% LV IMLT	
3947, 3804	3959, 3825,	3987, 3810, 3462	3924, 3888, 3398	O–H stretching in the carboxyl group
–	3199	3239	3167	NH_3^+ asymmetric stretching of L-valine
3009	2946	2895	2925	C–H asymmetric stretching vibration of carboxyl group
2842	2843	2843	2689	Presence of N–H functional group in the title compound
1680, 1584	1663, 1588	1696, 1592	1655	C = N stretching vibration of imidazole ring
1438	1435	1445	1464	characteristic peak of aromatic ring vibrations their
1334	1338	1335	1339	In-plane bending modes of aromatic C–H bonds
1303	1305	1316	1309	C = O stretching
1248	1263	1259	1267	The breathing mode of the imidazole ring in plane C–H deformation
1212	1213	1215	1213	C–H in plane of the aromatic ring
1128	1134	1154	1134	C–C stretching of imidazole
1091	1092	1059	1088	CO–OH stretching vibrations of carboxylate groups
879	842	854	867	C–C–N asymmetric stretching
791	788	794	777	C–H out of plane deformation
717	731	759	762	COO^- scissoring
642	654	698	678	The bending vibrations of COO^-
627	635	626	627	C–C deformation
491	504	519	522	N–C–N stretching

Fig. 11 Etch patterns of grown crystals **a** Pure IMLT, **b** 1 mol% LV doped IMLT, **c** 3 mol% LV doped, **d** 5 mol% LV doped IMLT



of etch pits are observed. This is expected to affect the quality of the crystal and hence its performance. The L-valine (3 mol %) doped IMLT crystal has the inclusion of air bubble in the crystal which shall reduce its efficiency.

3.7 Z-Scan analysis

The third order nonlinearity is responsible for the nonlinear optical (NLO) effects such as four-wave mixing phenomena [34]. The third order nonlinear optical phenomenon is associated with the intensity dependent change in the nonlinear refractive index and nonlinear absorption coefficient. Z-scan technology is a reliable technique to measure the nonlinear refractive index and absorption coefficient of the solid materials. The real and imaginary parts of the nonlinear susceptibility as well as their signs can be found by using the nonlinear refractive index and absorption coefficient. The term Z-scan is coined since the sample is scanned along the Z- direction. Samples having thickness less than the Rayleigh length are favorable for the study. The gaussian laser beam is focused by a lens and is allowed to pass through the sample which is moved along the beam direction by using a motorized translation stage. The sample exhibits self -focusing or self- defocusing nature due to the alteration of refractive index by the beam. A Gaussian laser beam of a continuous-wave (cw) generated with the wavelength of 532 nm from a frequency-converted diode-pumped Nd: YAG laser beam was projected on the single crystals to examine their third-order nonlinear optical (NLO) properties.

Using a stepper motor, the samples (grown crystals) are moved along the negative and positive z-axis with the simultaneous passage of the Gaussian laser beam focused on the samples [35]. The intensity of the incident cw-laser beam is varied by moving the grown crystal (sample) through the focal point of the lens. The grown crystal samples were placed in the focal point of the lens in the normalized transmittance condition and the intensities were recorded. This is carried out to maintain the intensity of the beam at a constant value. The normalized transmittance values of the samples were recorded in both the open and closed aperture modes and are presented in the Fig. 12a, b and c. The transmitted intensities from both the closed and open aperture methods are investigated and the nonlinear parameters are determined.

3.7.1 Closed aperture method

In the closed aperture method the laser beam is transmitted along the z- direction and the sample is moved along the direction of propagation of the laser beam. It is found that the intensity of the laser beam gets altered by the sample since its refractive index gets altered. The dependence of self-defocusing / self-focusing nature on the optical properties of the samples can be obtained. The samples having self-focusing nature possess pre-focal transmitted valley and then pos-focal transmitted peak which is attributed to the positive refractive index of the sample ($n_2 > 0$). The negative refractive index of the sample ($n_2 < 0$) was established due to the self- defocusing nature of the sample since a pre-focal transmitted peak followed by a post-focal transmitted valley are observed. The obtained data for the grown crystals is shown in Fig. 12a, which is recorded by exposing the grown crystals in the closed aperture Z-scan method. Through the closed aperture method, the self-defocusing character of grown crystals are confirmed since the data shows the existence of a transmitted peak trailed by a valley, which can be attributed to the local deviation in the refractive index [36]. To fabricate devices that function as optical sensors, it is preferred that the materials exhibit self-defocusing character.

The parameter $\Delta\phi$, the on-axis phase shift at the focal point is determined. The relationship between the third-order nonlinear refractive index (n_2) and the on-axis phase shift ($\Delta\phi$) are studied. The numerical values of nonlinear refractive index for the grown IMLT single crystals were determined and are depicted in Table 6.

3.7.2 Open aperture method

Open aperture Z-scan is a method employed to measure the nonlinear absorption coefficient (β) of samples. The value of β of a crystal may be positive or negative, and is found to vary due to the nature of interaction between the sample and the incident laser beam. In the open-aperture method, (placed in normalized transmittance curvature mode), a reverse saturable absorption curve is attained for samples exhibiting positive nonlinear absorption coefficient (β), and a negative value of nonlinear absorption coefficient (β) is exhibited by the crystals possessing the saturable absorption nature [37]. The saturable

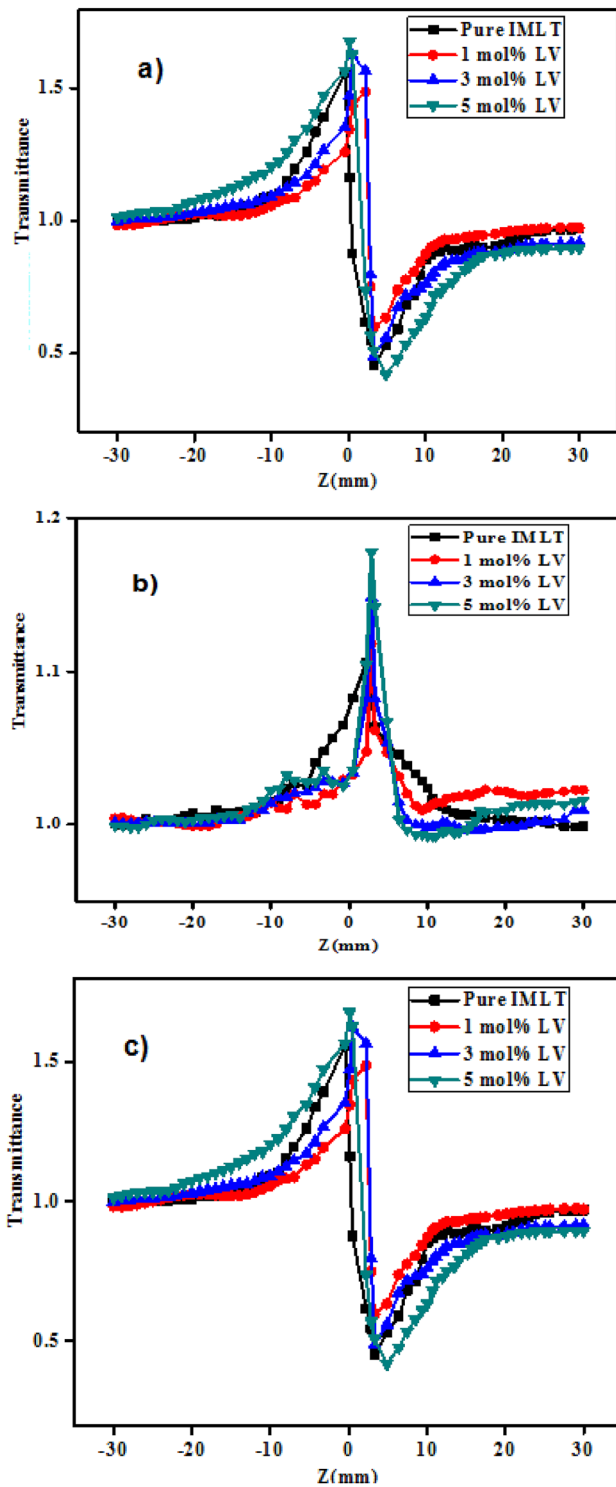


Fig. 12 **a** Z-scan-Closed aperture data of pure and L-valine doped IMLT crystals. **b** Open aperture Z-scan data of L-valine doped IMLT crystals. **c** Ratio of closed aperture data to open aperture Z-scan data

absorption behavior of the grown single crystals is confirmed from the obtained data presented in

Fig. 12b. The possessions of negative nonlinear absorption coefficient (β) of the grown crystals are proved. The obtainment of the value of ' β ' with a lesser degree of accuracy in the closed-aperture method is witnessed since the nonlinear refractive index and saturation absorption coefficient affect the transmittance of the single crystals. This signifies that it is imperative to distinguish the nonlinear absorption coefficient (β) from the transmitted nonlinear refractive index (n_2) values. The respective transmitted values (obtained from the closed aperture scan) are divided by open aperture scan and the information is shown in Fig. 12c.

The contributing real and imaginary factors of the 3rd order non-linear susceptibilities for the samples are calculated by employing the relations connecting them as presented below [38].

$$R_e(\chi^{(3)}) = \frac{10^{-4} \epsilon_0 C^2 n_0^2 n_2}{\pi} \left(\frac{cm^2}{W} \right) \tag{5}$$

$$I_m(\chi^{(3)}) = \frac{10^{-2} \epsilon_0 C^2 n_0^2 \lambda \beta}{4\pi^2} \left(\frac{cm}{W} \right) \tag{6}$$

The third-order nonlinear susceptibility of the grown crystals were calculated using the following relation.

$$\chi^{(3)} = \sqrt{(R_e(\chi^{(3)}))^2 + (I_m(\chi^{(3)}))^2} esu \tag{7}$$

And are tabulated in Table 6. L-valine doped IMLT single crystals have higher nonlinear optical susceptibility in the case of 1 mol % doping concentration, which elucidates the substantial distribution of the dopant atoms enabling the increment of the dipolar moment. Owing to the possession of self-defocussing nature in both the L-valine doped and un-doped IMLT single crystals, their suitability in the domains of sensor-operated devices and other optical applications are confirmed.

4 Conclusions

The powder XRD data implies the impact of dopant on the structural parameters of the un-doped IMLT single crystals are within a certain limit, and hence the crystal structure remains the same. The small variation is observed in lattice dimensions and strain was examined from powder XRD analysis. This confirms the amalgamation of the amino acid L-valine in the IMLT crystal. The crystallite size, strain

Table 6 Non-linear optical parameters of L-valine doped IMLT single crystals

Sample	$n_2 \cdot 10^{-8} \text{ cm}^2/\text{W}$	$\beta \cdot 10^{-4} \text{ cm/W}$	n_0	$\text{Re } \chi^{(3)} \cdot 10^{-6} \text{ esu}$	$\text{Im} \chi^{(3)} \cdot 10^{-6} \text{ esu}$	$\chi^{(3)} \cdot 10^{-6} \text{ esu}$
Pure IMLT	8.34	0.09	1.32	3.67	0.58	3.71
1 mol% LV	1.13	0.07	1.52	10.08	5.06	11.28
3 mol% LV	8.33	0.02	1.04	7.81	3.66	8.62
5 mol% LV	1.02	0.05	1.31	8.81	4.38	9.83

and dislocation densities were also calculated. L-valine doped IMLT has the largest crystallite size ($8.24 \times 10^{-8} \text{ m}$) having 1 mol % dopant concentration was found. The UV–Vis–NIR analysis unveils that the transparency of 1 mol% L-valine is high and it has large bandgap energy (4.82 eV) value which is an essential factor for the second-harmonic generation applications. The increase in the band gap of the doped crystals and the shift in the absorption coefficient towards the lower wavelength region show that the grown crystal can be utilized for photoconductive applications. The dielectric constant and dielectric loss factors for the grown crystals were measured. The dielectric measurement confirms that the L-valine (1 mol %) doped crystal has minimum heat dissipation factor and hence there is a minimum power loss. FTIR analysis confirms the vibrational groups present in the grown crystals. It is observed that the efficiency has increased while the doping concentration has increased till 1 mol%. It demonstrates that the 1 mol% L-valine doped crystal is suitable for the non-linear optical applications such as frequency conversion, second harmonic generation.

Acknowledgements

The corresponding author (Dr. R. Arun Kumar) places on record the gratitude to the South Eastern Regional Office (University Grants Commission), Hyderabad, India, for awarding the Minor research project (No.F. MRP-6721/16 (SERO UGC) Link 6721, dated 30 June 2017). The first author (Dr. P. Dhivya) is grateful to the PSG College of Technology for extending financial assistance to carry out this work (TEQIP/No A/17 dated 25 November 2017). Authors are also thankful to the authorities, NIT Andhra Pradesh for awarding SEED grant (Ref No. NITAP/SD—G/17/2020 dated 05/11/2020). Authors (Dr. R. Arun Kumar and Mr. Mitrabhanu Behera) thank

the funding received from Science Engineering and Research Board (SERB), Dept. of Science and Technology, Government of India (CRG/2020/002153 dated 25/12/2020).

Author contributions

The first author—PD has carried out the growth of single crystals reported herein as per the guidance of the corresponding author RAK. The second author MB had carried out the characterization and interpretation of the data along with the first author PD.

Funding

The authors have not disclosed any funding.

Data availability

The datasets generated during and/or analyzed during the current study are available from the corresponding author on reasonable request.

Declarations

Conflict of interest There are no competing interest among the authors in the manuscript submitted.

Ethical approval The authors confirm the fullest compliance with Ethical standards in the research work carried out.

References

1. H. Lin, JuXu. Bo Wang, R. Zhang, H. Chen, Yu. Yunlong, Y. Wang, Phosphor-in-glass for high-powered remote-type white AC-LED. *Appl. Mater. Interface* 6(23), 21264–21269 (2014)

2. P. Halappa, M.R. Harshitha, C. Shivakumara, Synthesis and structural characterization of orange red light emitting Sm³⁺ activated BiOCl phosphor for WLEDs applications. *J. Alloys Compd.* **785**, 169–177 (2019)
3. P. Halappa, A. Mathur, D. Marie-Helene, C. Shivakumara, Alkali metal ion co-doped Eu³⁺ activated GdPO₄ phosphors: structure and photoluminescence properties. *J. Alloys Compd.* **785**, 1086–1098 (2018)
4. J. Zhong, D. Chen, Y. Zhou, Z. Wan, M. Ding, W. Bai, Z. Ji, New Eu³⁺-activated perovskite La_{0.5}Na_{0.5}TiO₃ phosphors in glass for warm white light emitting diodes. *Dalton Transact.* **45**, 4762–4770 (2016)
5. J.D. Bierlein, H. Vanherzeele, Potassium titanyl phosphate: properties and new applications. *J. Optical Soc. Am. B* **6**, 622–633 (1989)
6. P.P. Fedorov, A.E. Kokh, N.G. Kononova, Barium borate b-BaB₂O₄ as a material for nonlinear optics. *Russian Chem. Rev.* **8**, 651–671 (2002)
7. R.F. Ali, B.D. Gates, Synthesis of lithium niobate nanocrystals with size focusing through an ostwald ripening process. *Chem. Matter.* **6**, 2028–2035 (2018)
8. C. Huang, F. Zhang, S. Pan, *Inorganic Nonlinear Optical Materials*. Reference Module in Chemistry, Molecular Sciences and Chemical Engineering (2022). <https://doi.org/10.1016/B978-0-12-823144-9.00081-9>
9. M. Divya Bharathi, G. Ahila, J. Mohana, R. Bhuvanewari, G. Anbalagan, Crystal growth and optical characterization of an organic single crystal for frequency conversion applications. *IOP Conf. Series* **360**, 012057 (2018)
10. L. Jothiac, G. Vasukib, R. Ramesh Babuc, K. Ramamurthi, Synthesis, crystal growth and characterization of organic NLO material: 4-Bromo-4'-hydroxybenzylidene aniline. *Optik* **125**, 2017–2021 (2014)
11. S.R. Thilagavathy, P. Rajesh, P. Ramasamy, K. Ambujam, 'Growth and characterization of pure and doped KHP NLO single crystals. *Spectrochimica Acta Part A* **127**, 248–255 (2014)
12. A. Miniewicz, Electro-optic investigations in some molecular-ionic crystals. *Mol. Cryst. Liquid Cryst. Sci. Technol. Sect. A. Mol. Cryst. Liquid Cryst.* **229**(1), 13–18 (1993)
13. M.S. Pandian, P. Ramasamy, Conventional slow evaporation and Sankaranarayanan-Ramasamy (SR) method grown diglycine zinc chloride (DGZC) single crystal and its comparative study. *J. Cryst. Growth* **312**(3), 413–419 (2010)
14. A. Choubey, O.P. Kwon, M. Jazbinsek, P. Günter, High-quality organic single crystalline thin films for nonlinear optical applications by vapor growth. *Cryst. Growth Des.* **7**(2), 402–405 (2007)
15. N. Kejalakshmy, K. Srinivasan, Electro-optic properties of potassium hydrogen phthalate crystal and its application as modulators. *J. Phys. D Appl. Phys.* **36**(15), 1778 (2003)
16. P. Dhivya, R. Arun Kumar, T. Theivasanthi, G. Vinitha, M. Kannan, Growth and characterization of a nonlinear optical material: l-histidine-doped imidazolium-tartrate. *Mater. Sci. J. Electron. Mater.* (2019). <https://doi.org/10.1007/s11664-019-07218-2>
17. P. Dhivya, R. Kumar, G. Vinitha, Investigations on the properties of L-proline doped imidazolium L-tartrate (IMLT) single crystals. *J. Mater. Sci.* (2021). <https://doi.org/10.1007/s10854-020-05113-9>
18. M. Prakash, D. Geetha, M.L. Caroline, P.S. Ramesh, Crystal growth, structural, optical, dielectric and thermal studies of an amino acid based organic NLO material: L-phenylalanine L-phenylalaniniummalonate. *Spectrochim. Acta Part A Mol. Biomol. Spectrosc.* **83**(1), 461–466 (2011)
19. M. Tabatabaee, M. Tahriri, M. Tahriri, Y. Ozawa, B. Neumüller, H. Fujioka, K. Toriumi, 'Preparation, crystal structures, spectroscopic and thermal analyses of two co-crystals of [M (H₂O) 6][M (dipic) 2] and (atrH) 2 [M (dipic) 2](M = Zn, Ni, dipic = dipicolinate; atr = 3-amino-1H-1, 2, 4-triazole) with isostructural crystal systems. *Polyhedron* **33**(1), 336–340 (2012)
20. P. Singh, M. Hasmuddin, M. Shakir, N. Vijayan, M.M. Abdullah, V. Ganesh, M.A. Wahab, Investigation on structural, optical, thermal, mechanical and dielectric properties of L-proline cadmium chloride monohydrate single crystals: an efficient NLO material. *Mater. Chem. Phys.* **142**(1), 154–164 (2013)
21. K. Thukral, N. Vijayan, Sonia, D. Haranath, K.K. Maurya, J. Philip, V. Jayaramkrishnan, Comprehensive study on l-proline lithium chloride monohydrate single crystal: a semiorganic material for nonlinear optical applications. *Arabian J. Chem.* **12**(8), 3193–3201 (2019)
22. P. Singh, M. Hasmuddin, N. Vijayan, M.M. Abdullah, M. Shakir, M.A. Wahab, Investigation on growth features and crystal structures of pure and metal ion (Mn²⁺) doped KDP single crystals. *Optik-Int. J. Light and Electron Opt.* **124**(13), 1609–1613 (2013)
23. M.K. Mohan, K. Jagannathan, S. Ponnusamy, C. Muthamizhchelvan, Effect of urea and thiourea on nonlinear optical hippuric acid crystals. *J. Phys. Chem. Solids* **72**(11), 1273–1278 (2011)
24. P. Dhivya, R. Arun Kumar, T. Theivasanthi, G. Vinitha, M. Kannan, D. Growth and characterization of a nonlinear optical material: L-histidine doped imidazolium L-tartrate (IMLT). *J. Electronic Mater.* **0361–5235**, 1–11 (2019)
25. K. Mohanraj, D. Balasubramanian, N. Jhansi, Structural, mechanical, electrical and optical properties of a new lithium

- boro phthalate NLO crystal synthesized by a slow evaporation method. *Opt. Laser Technol.* **96**, 318–322 (2017)
26. D. Sathya, V. Sivashankar, 'Growth and characterization of a new organic NLO crystal: guanidine acetate single crystals. *Optik-Int. J. Light Electron Optics* **126**(24), 5873–5876 (2015)
 27. T.P. Srinivasan, R. Indirajith, R. Gopalakrishnan, Growth and characterization of 1H-imidazolium hydrogen l-tartrate single crystals. *J. Crystal Growth* **312**(4), 542–547 (2010)
 28. M.R. Jagadeesh, H.S. Kumar, R.A. Kumari, Crystal growth and characterization of a new NLO crystal: urea 2-furoic acid. *Optik* **126**(23), 4014–4018 (2015)
 29. N. Elavarasu, S. Karuppusamy, S. Muralidharan, M. Anantharaja, R. Gopalakrishnan, 'Fabrication and performance study of electro-optical modulator and third order nonlinearity using unidirectional method (Sankaranarayanan–Ramasamy) grown Imidazolium l-Tartrate < 0 1 0 > single crystal. *Opt. Mater.* **46**, 141–148 (2015)
 30. G. Bhuvanewari, L.G. Prasad, N. Prabavathi, 'Crystal growth, experimental and theoretical investigations of organic NLO material 4-nitrophthalimide. *Optik* **166**, 307–316 (2018)
 31. F. Akhtar, J. Podder, A Study on structural, optical, electrical and etching characteristics of pure and l-alanine doped potassium dihydrogen phosphate crystals. *J. Crystallizat. Proc. Technol.* **1**(03), 55 (2011)
 32. S. Codato, R. Campi, C. Rigo, A. Stano, Ga assisted in situ etching of AlGaInAs and InGaAsP multi quantum well structures using tertiarybutylchloride. *J. Cryst. Growth* **282**(1–2), 7–17 (2005)
 33. A.H. Hameed, G. Ravi, R. Dhanasekaran, P. Ramasamy, Studies on organic indole-3-aldehyde single crystals. *J. Cryst. Growth* **212**(1–2), 227–232 (2000)
 34. M. Saravanan, T.C. SabariGirisun, G. Vinitha, S. VenugopalRao, Improved third-order optical nonlinearity and optical limiting behaviour of (nanospindle and nanosphere) zinc ferrite decorated reduced graphene oxide under continuous and ultrafast laser excitation. *RSC Adv.* **6**(94), 91083–91092 (2016)
 35. P.M. Dinakaran, G. Bhagavannarayana, S. Kalainathan, Synthesis, growth, structural, optical, spectral, thermal and mechanical studies of 4-methoxy 4-nitrostilbene (MONS): a new organic nonlinear optical single crystal. *Spectrochim. Acta Part A Mol. Biomol. Spectrosc.* **97**, 995–1001 (2012)
 36. P.V. Dhanaraj, N.P. Rajesh, J. Kalyana Sundar, S. Natarajan, G. Vinitha, Studies on growth, crystal structure and characterization of novel organic nicotiniumtrifluoroacetate single crystals. *Mater. Chem. Phys.* **129**(1–2), 457–463 (2011)
 37. T.C.S. Girisun, S. Dhanuskodi, G. Vinitha, χ (3) measurement and optical limiting properties of metal complexes of thiourea using Z-scan. *Mater. Chem. Phys.* **129**(1–2), 9–14 (2011)
 38. H.P. Li, C.H. Kam, Y.L. Lam, W. Ji, Femtosecond Z-scan measurements of nonlinear refraction in nonlinear optical crystals. *Opt. Mater.* **15**(4), 237–242 (2001)

Publisher's Note Springer Nature remains neutral with regard to jurisdictional claims in published maps and institutional affiliations.

Springer Nature or its licensor (e.g. a society or other partner) holds exclusive rights to this article under a publishing agreement with the author(s) or other rightsholder(s); author self-archiving of the accepted manuscript version of this article is solely governed by the terms of such publishing agreement and applicable law.